Proceedings of the 5th International Conference on Information Technology and Application in Biomedicine, in conjunction with
The 2nd International Symposium & Summer School on Biomedical and Health Engineering
Shenzhen, China, May 30-31, 2008

Segmentation of Brain Structures Using PET-CT Images

Yong Xia, *Associate Member IEEE*, Lingfeng Wen, *Member IEEE*, Stefan Eberl, *Member IEEE*,
Michael Fulham, and Dagan Feng, *Fellow, IEEE*

***Abstract*—The accurate segmentation of PET-only brain images is challenging because of the low spatial resolution and high noise level in PET data. PET/CT has now replaced PET and offers the opportunity to improve segmentation through the high resolution, lower noise CT data. This paper pioneers the research of PET-CT brain image segmentation, which takes advantage of the full information available from the combined scan. In the proposed approach, the contrast stretched CT image is utilized to delineate cerebrospinal fluid (CSF) from other brain tissues. Gray matter is separated from white matter by applying the fuzzy clustering of spatial patterns (FCSP) algorithm to the joint PET-CT image. We compared our approach to a widely used PET segmentation method in the SPM toolbox for simulation and patient data. Our results prove that the incorporation of anatomical information in CT images substantially improves the accuracy of brain structure delineation.**

I. Introduction

POSITRON emission tomography (PET) is able to detect subtle functional changes at the early stages of a disease process, which gives PET a distinct advantage over anatomical imaging techniques in the evaluation of neurodegenerative disorders [1]. However, the delineation of these subtle early changes can be operator-dependent. Computer-aided diagnosis, where segmentation is an essential step, offers the potential to reduce such bias.

A variety of segmentation approaches have been proposed [2], [3]. The SPM-based segmentation [4] is one of the more popular methods. This method, which we refer to as SPM-Seg in this paper, is based on cluster analysis with a modified mixture model and prior information about the likelihood of each voxel belonging to each of three major structures. However, due to the relatively low spatial resolution and intrinsic high noise level in PET data when compared to anatomical imaging such as CT and MR, it is challenging to accurately segment brain structures from PET data alone.

PET-CT scanning has essentially replaced PET in clinical practice. PET-CT scanners combine a PET scanner and a fast helical CT scanner in the one instrument, thus complementing functional imaging (PET) with co-registered anatomical imaging (CT). It would seem logical that the high resolution, lower noise CT structural information should aid segmentation of brain structures in PET-CT scans. However, until now, the segmentation of PET-CT brain images has not been addressed in the literature. Therefore, this research aims to investigate if the incorporation of the anatomical information in CT could really improve the performance of brain image segmentation. In this paper, we propose an approach to delineate three major brain structures - gray matter, white matter, and cerebrospinal fluid (CSF). We first applied contrast stretching to the CT image and then adopted the Otsu algorithm [6] and a region growing method [5] to differentiate CSF from other brain structures. We finally used the fuzzy clustering of spatial pattern (FCSP) algorithm [7] to further separate gray from white matter. We also compared our approach, which we refer to as the FCSP-Seg method, to the SPM-Seg algorithm on simulation and patient data.

II. Methods

A. Simulation and Patient PET/CT Data

The simulation was based on the Zubal anatomical phantom [10]. The PET sinogram data were simulated for an ECAT Exact HR+ scanner by the PET-SORTEO simulator [11] assuming FDG activity of 23.0 MBq in gray matter and 8.5 MBq in white matter. A 3D filtered back projection method was applied to derive reconstructed PET data with corrections of random, dead-time, attenuation and scatter.

The CT data was simulated based on the following CT image model [12]

$$CT(x,y,z) = K \cdot O(x,y,z) * PSF(x,y,z) + \Theta + \Phi \qquad (1)$$

where K is an energy-dependent contrast factor, $O(x,y,z)$ represents the 3D attenuation distribution of the scanned object, $PSF(x,y,z)$ is the point spread function (SPF) of the imaging system, Θ is noise, and Φ is other artifacts.

It was assumed that the attenuation value was uniform within the same tissue, the effect of PSF could be approximated by a Gaussian filter with the full width at half maximum (FWHM) of [4.4, 4.4, 4.2] mm for three dimensions, and the noise in each region followed a Gaussian distribution without contribution of other artifacts. The CT

Manuscript received February 29, 2008. This work was supported in part by ARC, PolyU/UGC grants and ISL/Australia-China special fund.

Dr Yong Xia, Dr Lingfeng Wen, A/Prof Stefan Eberl, Prof Michael Fulham, and Prof Dagan Feng are with the Biomedical and Multimedia Information Technology (BMIT) Research Group, School of Information Technologies, University of Sydney, Australia. (e-mail: y.xia@usyd.edu.au ; wenlf@ieee.org; feng@it.usyd.edu.au; stefan@cs.usyd.edu.au; mfulham@med.usyd.edu.au).

Dr Yong Xia, Dr Lingfeng Wen，Prof Dagan Feng are also with the Department of Electronic & Information Engineering, Hong Kong Polytechnic University, Hong Kong.

Dr Lingfeng Wen, A/Prof Stefan Eberl and Prof Michael Fulham are also with the Department of PET and Nuclear Medicine, Royal Prince Alfred Hospital, Sydney, Australia

Prof Michael Fulham is also with the Faculty of Medicine, University of Sydney, Australia.

simulation consists of the following three steps: (1) estimating the attenuation values of background, bones, gray matter, white matter, and CSF from clinical CT data; (2) convolving the attenuation volume with the 3D Gaussian filter; and (3) degrading each region with a zero-mean Gaussian noise, whose standard deviation is also derived from clinical CT data. The simulated CT data was generated in a matrix of $256\times256\times128$ with the voxel size of $1.1\times1.1\times1.4$ mm. The simulated PET data was then interpolated to the same voxel size as the CT data.

The clinical data were selected from the archives of the department of PET and Nuclear Medicine at Royal Prince Alfred Hospital and were acquired on a Biograph LSO Duo PET-CT scanner. The clinical MRI scans of the same patients were performed at Westmead Hospital.

B. Derivation of Image Priors

The spatial normalization function in the SPM toolbox [8] was used to estimate the 3D deformable transformation, which mapped the standard PET template to the patient PET data. The derived transformation was then applied to the standard image priors of brain mask, gray matter, white matter and CSF. The resultant image priors, which had the same dimension, location and 3D orientation as the patient data, were used to facilitate the segmentation.

C. Contrast Stretching of CT Images

Brain tissue occupies only a fairly small range (mostly within $[-10,160]$ Hounsfield Units (HU)) of the dynamic range of several thousand HU of CT images. To improve the contrast of brain tissue, the following intensity transformation to the brain region defined by the prior of brain mask was applied.

$$CT_T(x,y)=\begin{cases}0, & CT(x,y)<-10\\ H_{eq}[ct(x,y)], & -10\le CT(x,y)\le 160\\ 255, & CT(x,y)>160\end{cases} \quad (2)$$

where $CT(x,y)$ is the HU value at (x,y), $CT_T(x,y)$ is the intensity value of the transformed image, and the function $H_{eq}(\cdot)$ maps the intensity range $[-10,160]$ to $\{1,2,\cdots,254\}$ by using the histogram equalization technique [5].

After contrast stretching, those pixels whose intensity values fall in the set $\{1,2,\cdots,254\}$ were regarded as belonging to the brain and were then further processed.

D. Segmentation of CSF

CSF has a relatively high contrast from brain tissue in CT images, but in PET images it is difficult to distinguish CSF from white matter because of the partial volume effect (PVE) and because both tissues can have low tracer uptake on PET. Hence the delineation of CSF relied solely on the CT images.

To highlight the CSF region and suppress the noise amplified during the contrast stretching, the CT image was fused with the image prior of CSF as follows

$$CT_{HE}(x,y)=\left[Inv(CT_T(x,y))+\omega\cdot P_{CSF}(x,y)\right]/(1+\omega) \quad (3)$$

where $Inv(\cdot)$ represents the operator of inversing intensity, the prior $P_{CSF}(x,y)\in[0,255]$ is proportional to the probability of the pixel belongs to CSF, and the weight ω is set to be 0.5 in our experiments.

The fused image was thresholded by the Otsu algorithm [6] to produce a rough segmentation of CSF. However, due to the inaccuracy of the prior, the central part in the fused image is usually over emphasized and thus may result in larger CSF regions. To this end, those CSF regions in the central part were eroded by a disk with a radius of 3 pixels. Next, all obtained CSF regions were used as "seeds" and a region growing technique was adopted to achieve a refined segmentation. Finally, a 3×3 median filter was employed to remove the isolated small regions caused by noise.

E. Separation of gray matter from white matter

The region of gray matter and white matter has relatively low contrast and high noise level in both PET and CT images. Neither image alone can allow accurate separation of gray from white matter. Therefore, we applied the joint PET-CT information to the FCSP algorithm, which performs well when applied to data with low SNR [7].

In the FCSP algorithm, the pixel located at $s=(x,y)$ was characterized by a 2D spatial pattern $p_s=(PET(s),CT_T(s))$, which has a PET component and a CT component. The values of both components were normalized to the range $[0,255]$. The optimal segmentation was achieved by clustering all spatial patterns through minimizing the following objective function.

$$J_m(U,V)=\sum_{s\in S}\sum_{c=1}^{2}u_{cs}^m d_{cs}^2 \quad (4)$$

where S represents the region of gray matter and white matter, m is a fuzzy factor, u_{cs} is the membership of the pattern p_s to the cth cluster V_c, and d_{cs} is the dissimilarity between the pattern p_s and the prototype of V_c, which can be defined as

$$d_{cs}=d_{cs}^F+\alpha\cdot d_{cs}^S \quad (5)$$

where d_{cs}^F is the Euclidean distance between p_s and the center of V_c, d_{cs}^S is the spatial dissimilarity between p_s and V_c, and the weight α balances the contribution of two dissimilarity measures. The spatial dissimilarity d_{cs}^S characterizes how much of p_s's neighbourhood is occupied by other clusters and thus can be estimated as

$$d_{cs}^F=\frac{\left|\{p_t\in V_{1-c}\}\right|-\left|\{p_t\in V_c\}\right|}{\left|\{p_t\in V_{1-c}\}\right|+\left|\{p_t\in V_c\}\right|},\ t\in\eta_s \quad (6)$$

where η_s denotes the neighborhood of s and $|A|$ is the cardinality of set A.

The objective function can be minimized by performing the Picard iteration [9]. During initialization, half of the labels were randomly set and the others were set according to the priors of gray matter and white matter. To ensure the

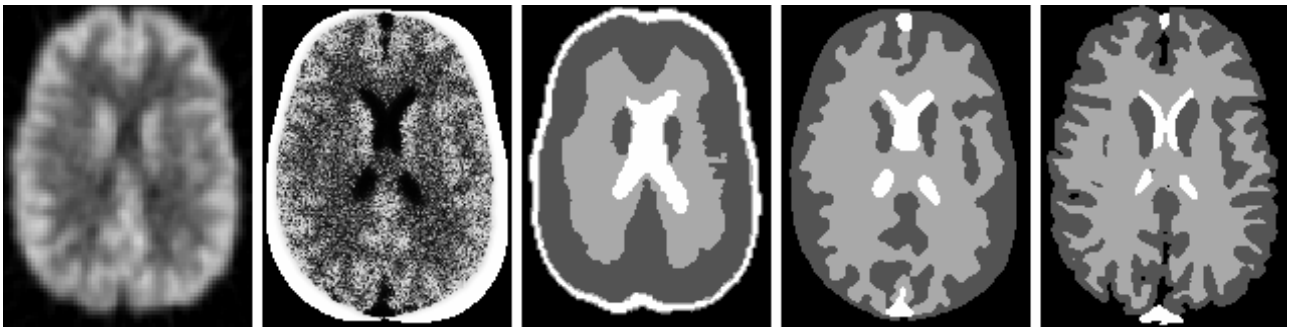

(a) (b) (c) (d) (e)

Fig. 1. Segmentation results on simulation data. (a) Simulated PET image, (b) Simulated CT image (after contrast stretching), (c) Result of SPM-Seg algorithm, (d) Result of the proposed FCSP-Seg algorithm, (e) Atlas

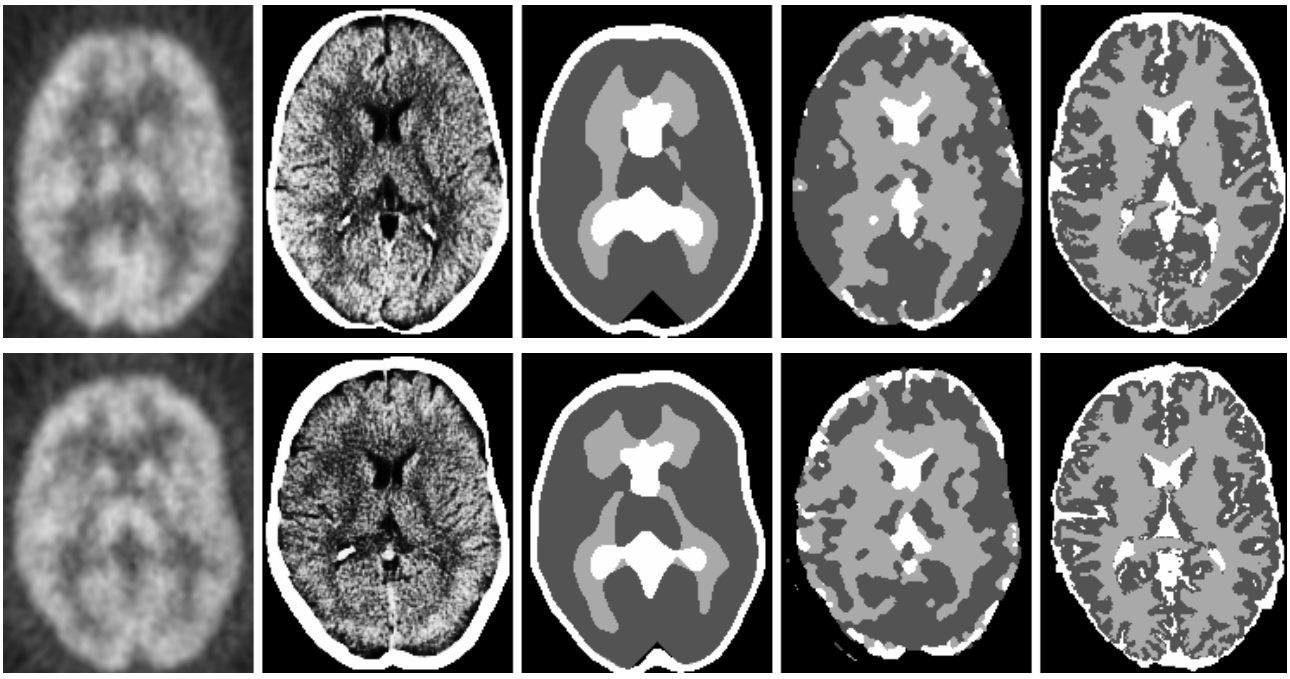

(a) (b) (c) (d) (e)

Fig. 2. Segmentation results on patient data. (a) Patient PET images, (b) Patient CT images (after contrast stretching), (c) Results of SPM-Seg algorithm, (d) Results of the proposed FCSP-Seg algorithm, (e) Reference images obtained by segmenting the MR images

optimization was dominated by intensity values in the early stage and by spatial constrains in the later stage, the following variable weight of dissimilarity was adopted

$$\alpha(n) = \alpha_0 \cdot \alpha_r^{(n)} \tag{7}$$

where n is the iteration number, α_0 and α_r are empirically initialized as 100 and 0.93.

III. Results

In this section, we compared the performance of the proposed FCSP-Seg approach with the SPM-Seg algorithm on both computer simulation and patient data.

The segmentation results obtained by applying both approaches to the 77th slice of PET-CT simulation data are given in Fig. 1. The segmentation performance was quantitatively assessed with the overlapping area measures of Dice similarity coefficient (DSC) [13]

$$DSC = 2\frac{|A_{Est} \cap A_{True}|}{|A_{Est}| + |A_{True}|} \tag{8}$$

where A_{Est} and A_{True} are the estimated area and true area, respectively. The DSC ranges from 0 to 1. $DSC = 1$ represents the optimal segmentation, where the estimated area is identical to the atlas in size, shape and location. The DSC values calculated on segmentation results of the 76th-79th slices are compared in Table I. It is obvious that the FCSP-Seg approach improves the segmentation performance significantly compared to the SPM-Seg algorithm.

TABLE I
PERFORMANCE COMPARISON ON SIMULATION DATA

Slice	Method	Gray Matter	White Matter	CSF
76th	SPM-Seg	0.603	0.600	0.300
	FCSP-Seg	0.792	0.835	0.759
77th	SPM-Seg	0.597	0.658	0.281
	FCSP-Seg	0.789	0.868	0.722
78th	SPM-Seg	0.588	0.668	0.229
	FCSP-Seg	0.776	0.861	0.630
79th	SPM-Seg	0.596	0.691	0.230
	FCSP-Seg	0.795	0.869	0.619

Next, the methods were evaluated on patient data. Fig. 2 compares the effectiveness of the SPM-Seg algorithm and the FCSP-Seg on two PET-CT slices taken from the clinical scans of two patients. Due to the lack of the correct diagnosis, the VBM5 toolbox [14] was applied to the co-registered MR image of the same patient and the segmentation result was used as a reference image. Based on the MR reference images, though the results of both methods are not satisfying, the proposed FCSP-Seg algorithm performs better than the SPM-Seg algorithm. A possible cause of the obvious difference between the PET-CT images and the MR images is that there is a considerable time interval between those two scans.

IV. CONCLUSION

This paper pioneers the research of automated segmentation of brain structures from PET-CT images. The proposed segmentation algorithm consists of three steps:- contrast stretching of the CT image, delineating CSF from other structures in the CT image, and differentiating gray from white matter by applying the FCSP algorithm to the joint PET-CT images. The comparative experiments on simulation and patient data suggest that our method is superior to the SPM-Seg method and provides more accurate segmentation results. This result proves that the incorporation of the anatomical information in CT images does substantially improve the performance of brain image segmentation. In the near future, we will extend this novel approach to the segmentation of 3D volume data with better accuracy and efficiency. We will also apply this approach to PVE correction and classification of neurological disorders.

ACKNOWLEDGMENT

The authors would like to thank Dr. Chong Wong at the Westmead Hospital, Sydney, Australia, for providing the MR images used in this study.

REFERENCES

[1] J.R. Petrella, R.E. Coleman, and P. M. Doraiswamy, "Neuroimaging and early diagnosis of Alzheimer Disease: A look to the Future," Radiology, vol. 226, no. 2, pp. 315-336, Feb. 2003.

[2] J. Mykkänen, M. Juhola, and U. Ruotsalainen, "Extracting VOIs from brain PET images," International Journal of Medical Informatics, vol. 58-59, pp. 51-57, Sep. 2000.

[3] J. Tohka, A. Kivimäki, A. Reilhac, J. Mykkänen, and U. Ruotsalainen, "Assessment of brain surface extraction from PET images using Monte Carlo simulations," IEEE Trans. on Nuclear Science, vol. 51, no. 5, pp. 2641-2648, 2004.

[4] J. Ashburner, and K.J. Friston, "Multimodal Image Coregistration and Partitioning - a Unified Framework," NeuroImage, vol. 6, pp. 209-217, 1997.

[5] R.C. Gonzalez, and R.E. Woods, Digital Image Processing (2nd ed.), Prentice Hall, Upper Saddle River, NJ, 2002.

[6] N. Otsu, "A threshold selection method from gray-level histograms," IEEE Trans. on Syst. Man Cybern., vol. SMC-9, no. 1, pp. 62–66, 1979.

[7] Y. Xia, D. Feng, T.J. Wang, R.C. Zhao, and Y.N. Zhang, "Image segmentation by clustering of spatial patterns," Pattern Recognit. Lett., vol. 28, no. 12, pp. 1548-1555, 2007.

[8] J. Ashburner, and K.J. Friston, "Nonlinear Spatial Normalization using Basis Functions," Human Brain Mapping, vol. 7, no. 4, pp. 254-266, 1999.

[9] J.C. Bezdek, Pattern Recognition with Fuzzy Objective Function Algorithms, Plenum Press, New York, 1981.

[10] I. G. Zubal, C. R. Harrell, E. O. Smith, Z. Rattner, G. Gindi, and P.B. Hoffer, "Computerized 3-dimensional segmented human anatomy," Med. Phys., vol. 21, pp. 299–302, Feb. 1994.

[11] A. Reilhac, G. Batan, C. Michel, C. Grova, J. Tohka, N. costes, and A.C. Evans, "PET-SORTEO: Validation and Development of database of simulated PET volumes," IEEE Trans. on Nucl. Sci., vol. 52, no. 5, pp. 46-52, 2005.

[12] W.A. Kalender, Computed Tomography (2nd ed.), Chapter 4, pp. 102-129, Publicis Erlangen, Germany, 2005.

[13] A.P. Zijdenbos, B.M. Dawant, R.A. Margolin, and A.C. Palmer, "Morphometric analysis of white matter lesions in MR images: Methods and validation," IEEE Trans. on Med. Imag., vol. 13, no. 4, pp. 716–724, Dec. 1994.

[14] J. Ashburner, and K.J. Friston, "Unified segmentation," Neuroimage, vol. 26, no. 3, pp. 839-851, 2005.